ACS APPLIED MATERIALS & INTERFACES

Research Article

www.acsami.org

Humidity-Sensing Properties of Urchinlike CuO Nanostructures Modified by Reduced Graphene Oxide

Zhenyu Wang,[†] Yan Xiao,[†] Xiaobiao Cui,[†] Pengfei Cheng,[†] Biao Wang,[‡] Yuan Gao,*[,†] Xiaowei Li,[†] Tianlin Yang,[†] Tong Zhang,[†] and Geyu Lu*[,†]

[†]State Key Laboratory on Integrated Optoelectronics, College of Electronic Science and Engineering, Jilin University, 2699 Qianjin Street, Changchun 130012, People's Republic of China

[‡]Changchun Institute of Optics, Fine Mechanics and Physics, Chinese Academy of Sciences, Dong Nanhu Road 3888, Changchun 130033, People's Republic of China

Supporting Information

ABSTRACT: Urchinlike CuO modified by reduced graphene oxide (rGO) was synthesized by a one-pot microwave-assisted hydrothermal method. The as-prepared composites were characterized using various characterization methods. A humidity sensor based on the CuO/rGO composites was fabricated and tested. The results revealed that the sensor based on the composites showed much higher impedance than pure CuO. Compared with the sensors based on pristine rGO and CuO, the sensor fabricated with the composites exhibited relatively good humidity-sensing performance in terms of response time and response value. The humidity-sensing mechanism was also briefly introduced. The enlargement of the impedance and improvement of the humidity-sensing properties are briefly explained by the Schottky junction theory.

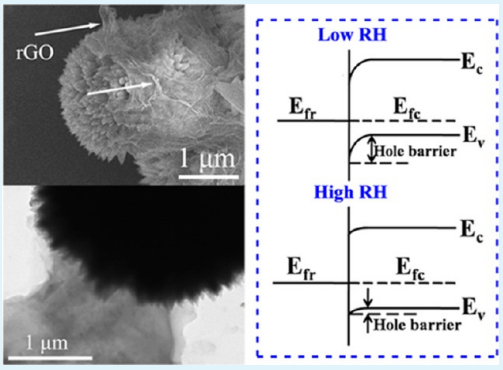

KEYWORDS: *urchinlike CuO, reduced graphene oxide, microwave-assisted hydrothermal, humidity sensor, Schottky junction theory*

INTRODUCTION

Graphene, a unique 2D carbon structure, because of its fascinating electronic, mechanical, thermal properties, and large specific surface areas,[1−4] has been considered to be a good candidate for many advanced technologies, such as nanoelectronics,[5] transparent conducting electrodes,[6] composites,[7] supercapacitors,[8] gas sensors,[9] and hydrogen storage.[10] Until now, there have been several available ways to prepare graphene, including mechanical exfoliation,[11] epitaxial growth,[12] chemical vapor deposition,[13] and chemically[14] or thermally[15] reduced graphene oxide (rGO). From the perspective of practical application, the most intensive attention has been paid to rGO, mainly because it can be produced on a large scale at a relatively low cost.[16]

Unfortunately, pristine rGO does not show ideal performances in some aspects. For instance, when applied in gas sensors, pristine rGO has exhibited poor sensing properties toward gases, including low sensitivity and irreversibility.[9] To improve the performances of pristine rGO, numerous modification methods have been tried, such as chemical functional groups modification,[17] a carbon nanotube/rGO hybrid,[18] noble metal particle decoration,[19,20] a polymer/rGO composite,[21] and metal oxides or metal sulfides/rGO composites.[22,23] As an important kind of functional materials, metal oxides have been widely used in many fields, for instance, field emitters[24−29] and gas sensors.[30,31] Because of the advantages of metal oxides and rGO, much attention has been paid to metal oxides/rGO composites. They combine the outstanding properties of metal oxides and rGO and might result in some particular properties because of the synergetic effect. To date, several kinds of metal oxides have been used to modify rGO, including ZnO,[32] Fe_2O_3,[33] NiO,[34] Co_3O_4,[35] TiO_2,[36] SnO_2,[37] Fe_3O_4,[38] Cu_2O,[39] and CuO.[40]

CuO, an important p-type semiconductor, has been used in many applications. Recently, the applications of CuO/rGO composites have also been reported. Significantly, in 2010, Mai et al.[41] reported a CuO/rGO composite obtained by an in situ chemical synthesis approach. When used as electrode materials for lithium ion batteries, the CuO/rGO composite ensured fast electron transfer between the active materials and collector and accommodated the volume expansion/contraction during discharge/charge process. Later, Zhao et al.[42] reported a leaflike porous CuO/rGO nanostructure synthesized by a hydrothermal method. Used as pseudo capacitor electrode materials, the nanostructures were found to exhibit superior performance in terms of specific capacitance and cyclability. In the next year, Sun and his cooperators reported a nonenzymatic glucose sensor based on a CuO/graphene-modified screen-printed carbon electrode integrated with flow-injection

Received: November 4, 2013
Accepted: January 23, 2014
Published: January 23, 2014

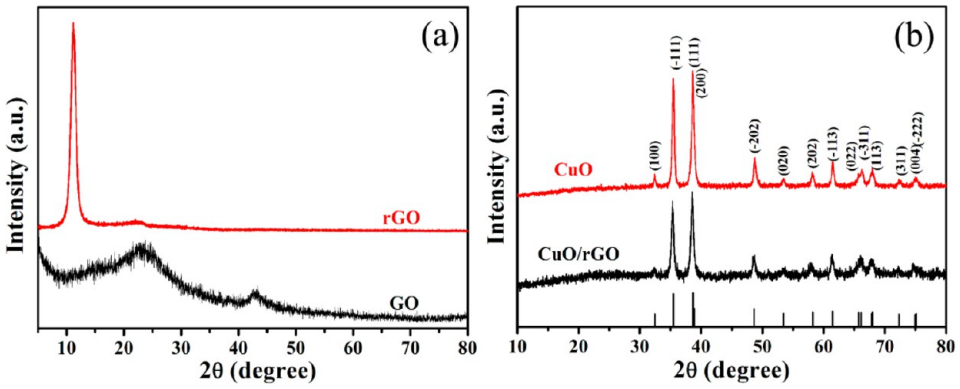

Figure 1. XRD patterns of GO and rGO (a) and CuO and CuO/rGO composites (b).

analysis.[43] It was found that the sensor showed an ultralow detection limit and high sensitivity.

Although CuO/rGO composites have been applied in some applications, there are few reports about their humidity-sensing properties. Herein, we report urchinlike CuO structures modified by rGO prepared by a microwave-assisted hydrothermal method. This method iffers from those synthesis methods in the literature, which reduced GO first. We obtained the composites by a simple one-pot method; the reduction of rGO and the synthesis of CuO were all in one step. The obtained CuO/rGO composites were then used to fabricate a humidity sensor. The testing results revealed that the sensor exhibited rapid response/recovery characteristics, high response value, and good repeatability. A sensing mechanism related to the Schottky junction model is proposed.

EXPERIMENTAL SECTION

Synthesis of Materials. Graphene oxide (GO) was synthesized from graphite powder according to the modified Hummer's method,[44] as shown in Supporting Information. CuO/rGO composites were prepared by a one pot microwave-assisted hydrothermal method. First, 1.5 mg of the obtained dry GO was ultrasonically redispersed into 40 mL deionized water, then 0.02 g of $CuCl_2{\cdot}2H_2O$ (Sinopharm Chemical Reagent Co. Ltd. China, 99%) was dissolved in the obtained dispersion by vigorous stirring for 20 min. After that, 0.04 g of urea (Sinopharm Chemical Reagent Co. Ltd. China, 99%) was added into the above solution under continuous stirring. Another 20 min later, the mixture suspension was then sealed in a 100 mL Teflon container and transferred into a microwave digestion system (Ethos One, Milestone incorporated). The reaction was conducted at 150°C for 30 min. After cooling to room temperature naturally, the precipitate was collected by centrifugation and washed by water and ethanol several times. After that, the obtained solid products were dried under ambient conditions overnight for further characterization and use. The urchinlike CuO structures were also prepared by a similar method without adding GO. For pristine rGO, the reaction was conducted under the same conditions without adding urea and $CuCl_2{\cdot}2H_2O$.

Fabrication and Testing of the Humidity Sensor. For fabricating the sensing devices, the paste was formed by mixing the products (rGO, CuO, and the composites) with ethanol then coated onto a ceramic substrate (10 mm × 5 mm, 0.5 mm thick) at a thickness of ~20 μm and dried in air at room temperature. The substrate was attached with Ag–Pd interdigitated electrodes, whose width and length were about 50 μm and 3.0 mm, respectively. The gap between adjacent counter electrodes was ~50 μm. The humidity-sensing properties were evaluated by an electrochemical interface and impedance/gain phase analyzer. A schematic diagram of the testing system is illustrated in Scheme S1 in the Supporting Information. Controlled humidity environments were obtained using saturated salt aqueous solutions in a closed glass vessel: LiCl, $MgCl_2$, NaBr, NaCl, KCl, and K_2SO_4, which yielded 11%, 33%, 59%, 75%, 85% and 98% relative humidity (RH), respectively. To maintain a constant RH, the temperature of the testing environment was maintained at 25°C. The response was defined as the ratio of the impedance in 11% RH to that in 98% RH. The time taken by the sensors to achieve 90% of the total complex impedance change from 11% to 98% RH was defined as the response time in the case of adsorption or the recovery time in the case of desorption from 98% to 11% RH.

Characterizations of Materials. Microwave-assisted hydrothermal reaction was conducted in a microwave digestion system (Ethos One) manufactured by Milestone Incorporated. X-ray power diffraction (XRD) analysis was conducted on a Rigaku D/max-2500 X-ray diffractometer with Cu Kα1 radiation (λ = 0.15406 nm), and the scanning speed was 12°/min. Field emission scanning electron microscopy (SEM) images were recorded on a JEOL JSM-7500F microscope operating at 15 kV. Transmission electron microscopy (TEM) and high-resolution transmission electron microscopy (HRTEM) images were obtained on a JEOL JEM-200EX microscope with accelerating voltage of 200 kV. Raman spectrum analysis was conducted on a Renishaw inVia Micro-Raman spectrometer. The X-ray photoelectron spectroscopy (XPS) data were determined on an ESCALAB 250 spectrometer. The humidity-sensing properties were evaluated by an electrochemical interface and impedance/gain phase analyzer (Solartron SI 1278 and SI 1260). Thermogravimetric (TG) analysis and differential scanning calorimetric (DSC) measurements were carried out using a NETZSCH STA 449F3 simultaneous thermogravimetric analyzer under air atmosphere from 30 to 800°C with a heating rate of 10°C min^{-1}.

RESULTS AND DISCUSSION

Materials Characterizations. Figure 1 shows the XRD patterns of the as-prepared GO, rGO, CuO, and CuO/rGO composites. The diffraction peak at around 2θ = 11.2° in Figure 1a belongs to the (001) reflection of GO. Using the Scherrer equation, the interlayer spacing of GO was 0.79 nm, much larger than that of pristine graphite (0.34 nm). The increase in the interlayer spacing can be attributed to the introduction of oxygen-containing functional groups on the graphite sheet surfaces.[45] For the rGO sample, two characteristic diffraction peaks can be observed at 23.5 and 42.8°, corresponding to the (002) and (100) planes of graphene. Figure 1b illustrates the XRD patterns of CuO and CuO/rGO composites. All the peaks in the spectra can be assigned to monoclinic CuO (a = 4.69270 Å, b = 3.42830 Å, c = 5.13700 Å, β = 99.546°, JCPDS Card No. 80-1916). None of obvious typical peaks belonging to rGO are observed in the XRD spectra of CuO/rGO composites. It can be ascribed to the low amount and low diffraction intensity of rGO. In addition, the CuO/rGO composites show a lower diffraction peak intensity than the pure CuO, suggesting that the CuO in the CuO/rGO composites has relatively low

crystallinity, owing to the high density of oxygen functional groups, including carboxylic, hydroxyl, and epoxy groups, on the GO surface to hinder diffusion and crystallization of CuO grains.[41]

Raman spectra of GO, rGO, and CuO/rGO composites are illustrated in Figure 2. As can be seen, all three materials show a

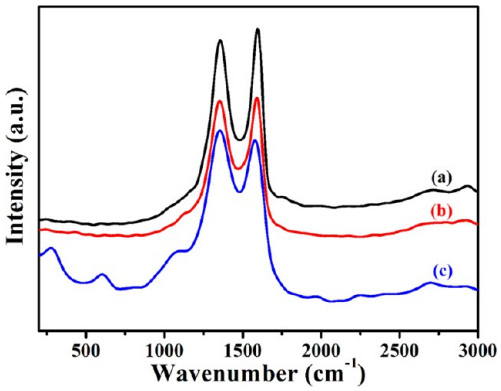

Figure 2. Raman spectra of GO (a), rGO (b), and CuO/rGO composites (c).

peak around 1354 cm^{-1}. It can be attributed to the D band associated with the structural defects that are related to the partially disordered structures of graphitic domains or created by the attachments of functional groups on the carbon basal plane. The peaks at 1595 (a), 1590 (b), and 1579 cm^{-1} (c) correspond to the G band, which arises from the first-order scattering of the E_{2g} phonon of the sp^2 C atoms.[46] Similar to the previous work, red shifts of the G band also can be observed in panels b and c.[47] It is also found that, after microwave-assisted hydrothermal treatment, the products show relatively higher intensity of the D to G band (1.10 for CuO/rGO composites and 1.00 for rGO) than that of GO (0.95). These observations confirm the formation of new graphitic domains after the heat treatment process.[46] In the spectrum of CuO/GO composites, there are two Raman peaks at 276 and 603 cm^{-1}, and these peaks can be assigned to the A_g and B_g modes of monoclinic CuO, respectively.[48]

The surface composition and element analysis for the resulting products were characterized by an XPS technique. Figure 3 shows the XPS spectra of GO, rGO, and the composites, all revealing two peaks at 285.5 and 531.0 eV, which are attributed to C 1s and O 1s, respectively. The other

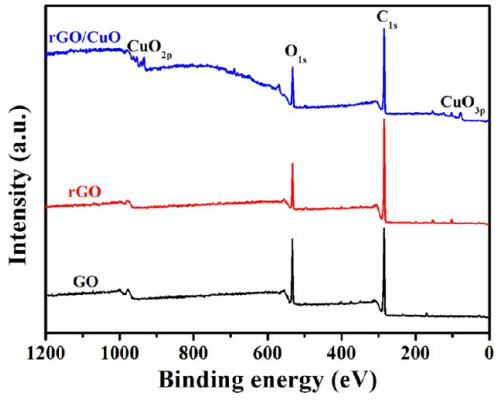

Figure 3. XPS spectra of GO, rGO, and rGO/CuO.

two peaks at 933.3 and 77.0 eV are also observed on the spectrum of the composites, which are associated with Cu 2p and Cu 3p, respectively.[49]

Figure 4 shows the C 1s spectra of GO, rGO, and the composites. The C 1s spectra could be deconvoluted into three peaks at 284.5, 286.6, and 288.4 eV, which are associated with C−C, C−O, and C═O, respectively. It is obviously seen that the peak intensity of C−O and C═O is strong in GO (Figure 4a); in contrast, after hydrothermal treatment, the peak intensity of C−O and C═O in the products tremendously reduces (Figure 4b and c). All the observations suggest that most of the oxygen-containing functional groups are successfully removed after hydrothermal treatment.[46]

The weight ratio of rGO and CuO was evaluated by a thermogravimetric analysis; the result is shown in Figure 5. As can be seen from the TG curve, the mass loss in the range of 30−300°C can be attributed to the loss of water. The remarkable mass loss from 300 to 500°C is ascribed to the decomposition of residual oxygen-containing groups and carbon oxidation from rGO. On the basis of the total weight loss of the CuO/rGO composites, the weight ratio of graphene in the composites was 8.6 wt %.

The morphologies of CuO and CuO/rGO composites were characterized with TEM and SEM analyses. As can be seen, the urchinlike structures are about 2 μm in diameter. There are some flakelike structures along with the urchinlike structures in pure CuO. To investigate them in detail, HRTEM analysis was conducted. A typical TEM image and a corresponding HRTEM image of a "flake" are shown in Figure S1 in the Supporting Information. From the HRTEM image, we can calculate the lattice spacing was 0.23 nm, which corresponds to the d spacing of the (111) crystal planes of monoclinic CuO, indicating the flakelike structures were CuO. On the basis of the SEM and TEM analysis, we can see that the CuO architectures in the composites are more uniform and compact. So it can be concluded that the existence of GO really has effects on the diffusion and crystallization of the CuO grains, as is discussed above. From the typical SEM and TEM images of the composites (Figure 6e, f) we can see that rGO shows a crumpled layered structure with some stacking layers. In addition, it can be observed that the rGO and CuO connect well with each other. To determine how rGO was distributed in the composites, a SEM image with low magnification of the composites is shown in Figure S2 in the Supporting Information. As can be seen, rGO was distributed randomly in the composites.

Humidity-Sensing Performances. As is well known, the responses of humidity sensors are dependent on the testing frequency. To investigate the humidity-sensing properties, the testing frequency should be determined first. Hence, the impedances of the sensors based on rGO, CuO, and CuO/rGO composites at different RHs were tested with different testing frequencies. The results are shown in Figure 7. As can be seen, regardless the frequency, the impedances of pristine rGO did not change obviously when the RH rose from 11% to 98%, indicating that rGO showed extremely small responses to humidity. For CuO, the impedances decreased with an in crease in the humidity, showing a nearly linear curve and the largest response when measured at 10 Hz. The response was 227.7; this small value makes it have poor precision for determining humidity, thus hindering its application. Under all three frequencies, the impedances of CuO/rGO composites changed relatively less at the low humidity range (11−59%). When the

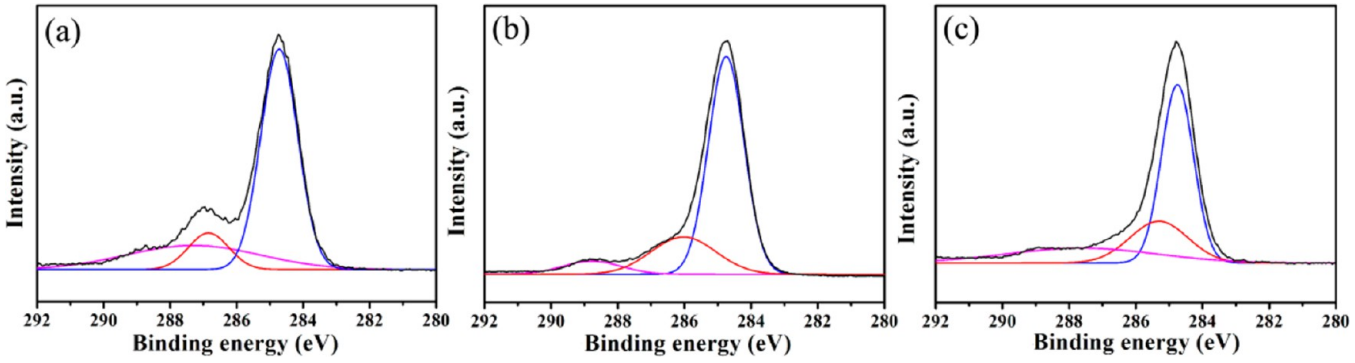

Figure 4. C 1s spectra of GO (a), rGO (b), and rGO/CuO (c).

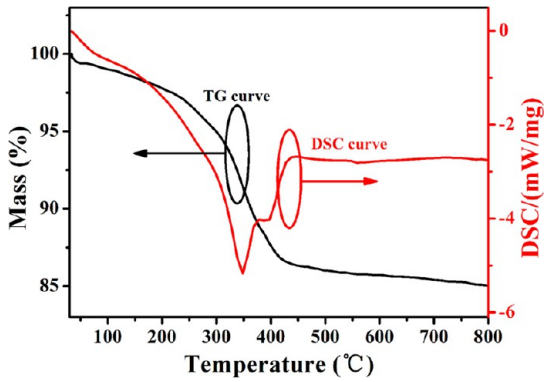

Figure 5. TG and DSC curves of the as-synthesized CuO/rGO composites.

RH rose to the high range (75–98%), the impedances decreased a lot. The highest response of the composites was about 22 700 (measured at 10 Hz). On the basis of the obtained results, 10 Hz was chosen to be the testing frequency. Furthermore, working at high RH, the composites showed high response, so they might be able to more accurately detect the humidity, much easier to avoid the interference of external factors, such as circuit noise. So the composites may have much better application prospects than pure CuO as a humidity-sensing material.

Figure 8 shows the response and recovery curves of CuO (a) and CuO/rGO composites (b) measured at 10 Hz when RH alternately changes between 11% and 98%. As can be seen, both pristine CuO and the composites showed good repeatability and rapid response/recovery characteristics. The response/recovery times for CuO and the composite are 10/16 and 2/17 s, respectively. Compared with those humidity sensors in the literature,[50−52] the sensor based on the CuO/rGO composite showed a faster response/recovery process. What is more, the composites show better repeatability than pure CuO, which is an important parameter for a humidity sensor. So we can conclude that the sensor based on the composites shows good performance when working under relatively high RH. Current−voltage (I−V) curves of pristine CuO and the composites under different RHs are shown in Figure S3 in the Supporting Information. It can be seen that the slope of the I−V curves increased with an increase in the RH.

Discussions of the Sensing Mechanism. The electrical response occurring in a humidity sensor must be linked to the water adsorption process taking place on the exposed surface of the sensing material.[53−56] The adsorbed water molecules can be divided into two kinds: chemisorbed and physisorbed. The initial layer is chemisorbed; once formed, it is not further affected by exposure to humidity and is difficult to remove. With the addition of humidity, physisorbed layers would form upon the chemisorbed layer. They are easily removed by decreasing the humidity. At a lower RH, the charge transport is

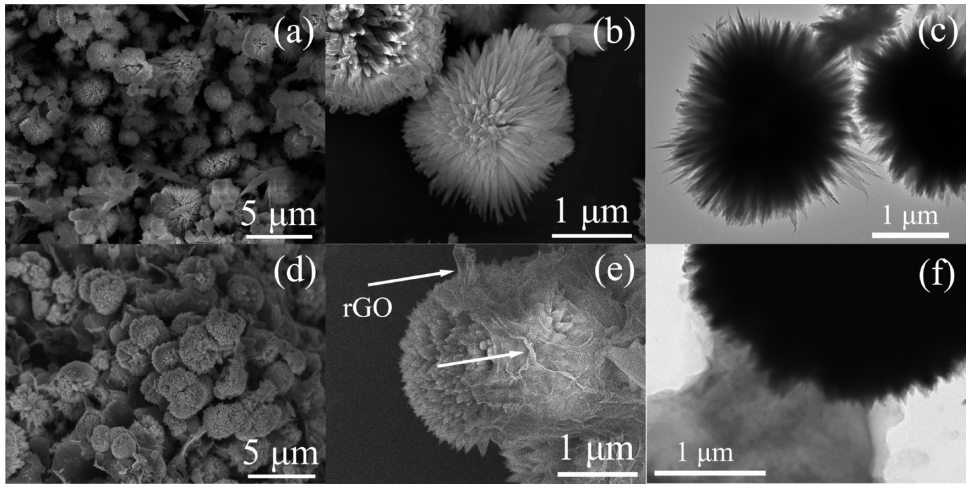

Figure 6. SEM images of CuO (a, b) and CuO/rGO composites (d, e); typical TEM images of CuO urchins (c) and an rGO−CuO junction (f). White arrows in part e indicate the rGO sheets.

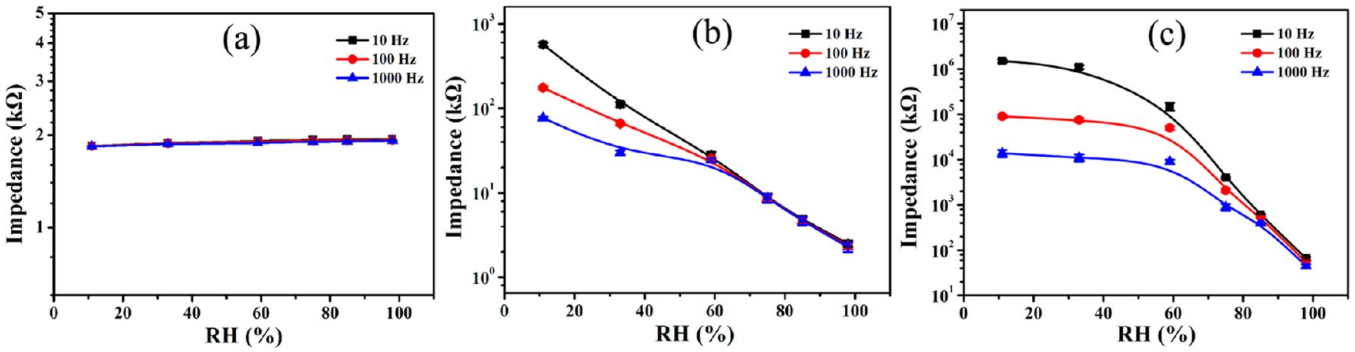

Figure 7. Impedances of the sensors based on rGO (a), CuO (b), and the composites (c) under different RHs measured at different frequencies.

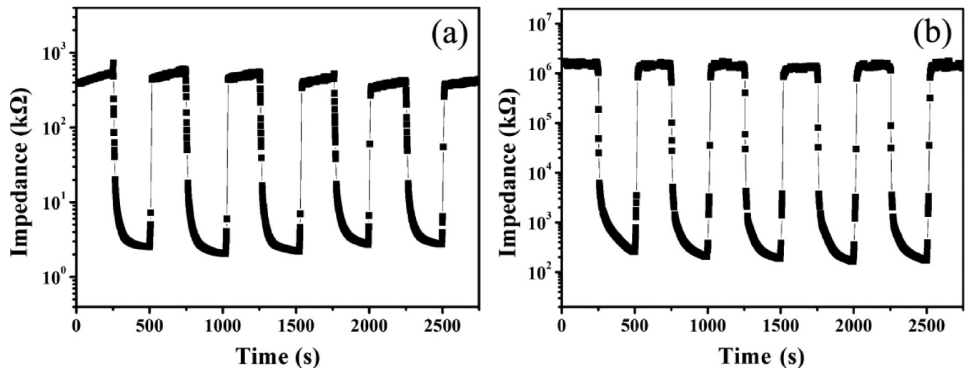

Figure 8. Response and recovery properties of the sensors fabricated with CuO (a) and the composites (b). The curves were measured between 11% and 98% RH at 25°C.

Scheme 1. Schematic Diagram of the Capillary Condensation Phenomenon on the Surface of Urchinlike CuO (a) and Energy Band Diagram of a CuO/rGO Schottky Junction under Low (b) and High (c) RH

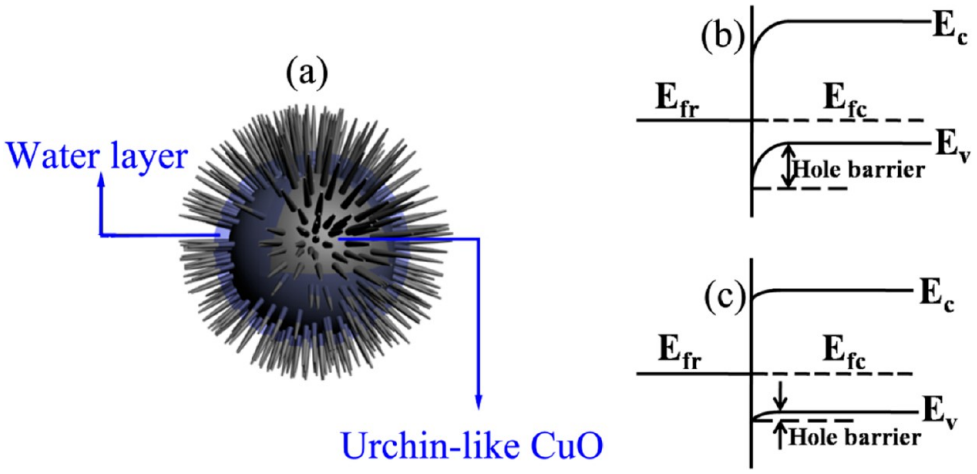

secured by proton hopping between chemisorbed hydroxyl groups. Afterward, when the amount of physisorbed water molecules starts to appear, the hydronium ion, H_3O^+, is most likely the charge carrier. Further, at higher RH, this probably occurs by the Grotthus transport mechanism.[30] At higher humidity levels, physisorbed water layers show a liquidlike behavior, and H^+ ions move freely.

The humidity response of CuO could be explained by the above humidity-sensing mechanism. Furthermore, the pores formed in the gap of the spines on urchinlike CuO may facilitate the capillary condensation at a lower RH level to give rise to a higher impedance response for humidity-sensing.[57] A schematic diagram for this phenomenon is shown in Scheme 1a.

rGO is a kind of good conductor; CuO is a p-type semiconductor. The work function of thin graphene layers and CuO is ~4.6 and 5.2 eV,[58,59] respectively. Similar to other kinds of semiconductors (TiO_2,[60,61] ZnO,[62] SnO_2,[63] CdS,[64] Si,[65] and WO_3[66]), when CuO is well connected with rGO, a Schottky junction will be formed, as shown in Scheme 1b.

Because of the good conductivity and ultralow humidity sensitivity, other than forming Schottky junctions, rGO has little contribution to the impedance of the composites. The impedance of the composites is determined by mainly three parts: first, the surface impedance of CuO; second, the bulk

impedance of CuO; and third, the impedance of rGO−CuO Schottky junctions (responsible for the larger impedance of the composites than pure CuO). Therefore, the impedance change in the composites caused by humidity change was also determined by the above three parts. When the relative humidity increased, the water molecules would cause the surface electric impedance of CuO to rise by increasing electron concentration (decreasing hole concentration) in two ways: first, the water molecules substituted for the absorbed oxygen ions and released electrons back to CuO; and second, the absorbed water molecules would attract electrons to the surface of CuO.

Similar to CuO, under low humidity conditions, charge transport occurred by the hopping mechanism, decreasing the surface impedance. The adsorption and desorption took place only on the surface of the CuO, so the bulk impedance of the CuO did not changed significantly with a change in the humidity. For the rGO−CuO Schottky junction, because of the injection of electrons, the work function of the CuO decreased, as shown in Scheme 1c, so the hole barrier decreased simultaneously, causing the electric impedance decrease in the Schottky junctions. With increasing humidity levels, water was physisorbed onto the top of the chemisorbed layer. Conduction probably occurs by the Grotthus transport mechanism, so the protons could migrate more easily, and the surface impedance of CuO decreased sharply. At the same time, the elevated humidity further decreased the hole barrier, reducing the impedance of the Schottky junctions greatly. Eventually, the impedance of the composites changed greatly under high humidity conditions, showing a high response to humidity. It is necessary to notice that when the adsorbed water layers were far from the CuO surface, it was difficult for the upper water molecules to attract electrons. Thus, when the humidity was raised to a certain level, the hole concentration of the surface and the hole barrier would not have obviously changed along with the increase in the humidity. The impedance of the composites was determined by the migration of the protons on the CuO surface. The sensor based on the composites showed a smaller response under low humidity conditions. This phenomenon can be explained as follows: Under lower humidity conditions, the protons' hopping and the hole barrier reduction decreased the impedance, but because of the existence of the hole barrier, the decrease in the impedance was not obvious when comparing with the initial impedance.

CONCLUSION

Urchinlike CuO nanostructures modified by rGO was synthesized by a one-pot microwave-assisted hydrothermal method. The sensors based on the as-prepared CuO/rGO composites showed good characteristics relative to humidity, including high response, a rapid response/recovery process, and good reproducibly. The improved humidity-sensing properties were also briefly explained by the Schottky theory.

ASSOCIATED CONTENT

Supporting Information

Schematic diagrams of the humidity-sensing system; preparation of GO; a typical TEM image and the corresponding HRTEM image of a "flake" structure; a SEM image of the composites with low magnification, and $I-V$ curves of pristine CuO and the composite under different RH. This material is available free of charge via the Internet at http://pubs.acs.org.

AUTHOR INFORMATION

Corresponding Authors

*E-mail: gaoyuan@jlu.edu.cn.
*E-mail: lugy@jlu.edu.cn.

Notes

The authors declare no competing financial interest.

ACKNOWLEDGMENTS

This work was supported by Natural Science Foundation of China (Nos. 61304242, 61327804, 61074172, 61134010), China Postdoctoral Science Foundation (No. 2013M530979), and Program for Changjiang Scholars and Innovative Research Team in University (No. IRT1017).

ABBREVIATIONS

rGO, reduced graphene oxide
GO, graphene oxide
RH, relative humidity
XRD, X-ray power diffraction
SEM, scanning electron microscopy
TEM, transmission electron microscopy
HRTEM, high resolution transmission electron microscopy
XPS, X-ray photoelectron spectroscopy
TG, thermogravimetric
DSC, differential scanning calorimetric

REFERENCES

(1) Novoselov, K. S.; Geim, A. K.; Morozov, S. V.; Jiang, D.; Zhang, Y.; Dubonos, S. V.; Grigorieva, I. V.; Firsov, A. A. Electric Field Effect in Atomically Thin Carbon Films. *Science* **2004**, *306* (5696), 666−669.
(2) Geim, A. K.; Novoselov, K. S. The Rise of Graphene. *Nat. Mater.* **2007**, *6* (3), 183−191.
(3) Lee, C.; Wei, X.; Kysar, J. W.; Hone, J. Measurement of the Elastic Properties and Intrinsic Strength of Monolayer Graphene. *Science* **2008**, *321* (5887), 385−388.
(4) Balandin, A. A.; Ghosh, S.; Bao, W.; Calizo, I.; Teweldebrhan, D.; Miao, F.; Lau, C. N. Superior Thermal Conductivity of Single-Layer Graphene. *Nano Lett.* **2008**, *8* (3), 902−907.
(5) Berger, C.; Song, Z.; Li, T.; Li, X.; Ogbazghi, A. Y.; Feng, R.; Dai, Z.; Marchenkov, A. N.; Conrad, E. H.; First, P. N.; de Heer, W. A. Ultrathin Epitaxial Graphite: 2D Electron Gas Properties and a Route toward Graphene-Based Nanoelectronics. *J. Phys. Chem. B* **2004**, *108* (52), 19912−19916.
(6) Bae, S.; Kim, H.; Lee, Y.; Xu, X.; Park, J. S.; Zheng, Y.; Balakrishnan, J.; Lei, T.; Ri Kim, H.; Song, Y. I.; Kim, Y. J.; Kim, K. S.; Ozyilmaz, B.; Ahn, J. H.; Hong, B. H.; Iijima, S. Roll-to-Roll Production of 30-inch Graphene Films for Transparent Electrodes. *Nat. Nano* **2010**, *5* (8), 574−578.
(7) Stankovich, S.; Dikin, D. A.; Dommett, G. H. B.; Kohlhaas, K. M.; Zimney, E. J.; Stach, E. A.; Piner, R. D.; Nguyen, S. T.; Ruoff, R. S. Graphene-Based Composite Materials. *Nature* **2006**, *442* (7100), 282−286.
(8) Yoo, J. J.; Balakrishnan, K.; Huang, J.; Meunier, V.; Sumpter, B. G.; Srivastava, A.; Conway, M.; Mohana Reddy, A. L.; Yu, J.; Vajtai, R.; Ajayan, P. M. Ultrathin Planar Graphene Supercapacitors. *Nano Lett.* **2011**, *11* (4), 1423−1427.
(9) Yuan, W.; Liu, A.; Huang, L.; Li, C.; Shi, G. High-Performance NO_2 Sensors Based on Chemically Modified Graphene. *Adv. Mater.* **2013**, *25* (5), 766−771.
(10) Dimitrakakis, G. K.; Tylianakis, E.; Froudakis, G. E. Pillared Graphene: A New 3-D Network Nanostructure for Enhanced Hydrogen Storage. *Nano Lett.* **2008**, *8* (10), 3166−3170.
(11) Dan, Y.; Lu, Y.; Kybert, N. J.; Luo, Z.; Johnson, A. T. C. Intrinsic Response of Graphene Vapor Sensors. *Nano Lett.* **2009**, *9* (4), 1472−1475.

(12) Emtsev, K. V.; Speck, F.; Seyller, T.; Ley, L.; Riley, J. D. Interaction, Growth, and Ordering of Epitaxial Graphene on SiC{0001} Surfaces: A Comparative Photoelectron Spectroscopy Study. *Phys. Rev. B* **2008**, *77* (15), 155303.
(13) Reina, A.; Jia, X.; Ho, J.; Nezich, D.; Son, H.; Bulovic, V.; Dresselhaus, M. S.; Kong, J. Large Area, Few-Layer Graphene Films on Arbitrary Substrates by Chemical Vapor Deposition. *Nano Lett.* **2008**, *9* (1), 30−35.
(14) Moon, I. K.; Lee, J.; Ruoff, R. S.; Lee, H. Reduced Graphene Oxide by Chemical Graphitization. *Nat. Commun.* **2010**, *1*, 73.
(15) Lu, G.; Ocola, L. E.; Junhong, C. Gas Detection Using Low-Temperature Reduced Graphene Oxide Sheets. *Appl. Phys. Lett.* **2009**, *94* (8), 083111−083111-3.
(16) Dong, Z.; Jiang, C.; Cheng, H.; Zhao, Y.; Shi, G.; Jiang, L.; Qu, L. Facile Fabrication of Light, Flexible and Multifunctional Graphene Fibers. *Adv. Mater.* **2012**, *24* (14), 1856−1861.
(17) Zhao, G.; Jiang, L.; He, Y.; Li, J.; Dong, H.; Wang, X.; Hu, W. Sulfonated Graphene for Persistent Aromatic Pollutant Management. *Adv. Mater.* **2011**, *23* (34), 3959−3963.
(18) Li, Y. F.; Liu, Y. Z.; Yang, Y. G.; Wang, M. Z.; Wen, Y. F. Reduced Graphene Oxide/MWCNT Hybrid Sandwiched Film by Self-Assembly for High Performance Supercapacitor Electrodes. *Appl. Phys. A* **2012**, *108* (3), 701−707.
(19) Xu, S.; Yong, L.; Wu, P. One-Pot, Green, Rapid Synthesis of Flowerlike Gold Nanoparticles/Reduced Graphene Oxide Composite with Regenerated Silk Fibroin As Efficient Oxygen Reduction Electrocatalysts. *ACS Appl. Mater. Interfaces* **2013**, *5* (3), 654−662.
(20) Li, Y.; Tang, L.; Li, J. Preparation and Electrochemical Performance for Methanol Oxidation of Pt/Graphene Nanocomposites. *Electrochem. Commun.* **2009**, *11* (4), 846−849.
(21) Pham, V. H.; Dang, T. T.; Hur, S. H.; Kim, E. J.; Chung, J. S. Highly Conductive Poly(methyl methacrylate) (PMMA)-Reduced Graphene Oxide Composite Prepared by Self-Assembly of PMMA Latex and Graphene Oxide through Electrostatic Interaction. *ACS Appl. Mater. Interfaces* **2012**, *4* (5), 2630−2636.
(22) Li, Y.; Wang, H.; Xie, L.; Liang, Y.; Hong, G.; Dai, H. MoS_2 Nanoparticles Grown on Graphene: An Advanced Catalyst for the Hydrogen Evolution Reaction. *J. Am. Chem. Soc.* **2011**, *133* (19), 7296−7299.
(23) Zhu, J.; Zhu, T.; Zhou, X.; Zhang, Y.; Lou, X. W.; Chen, X.; Zhang, H.; Hng, H. H.; Yan, Q. Facile Synthesis of Metal Oxide/Reduced Graphene Oxide Hybrids with High Lithium Storage Capacity and Stable Cyclability. *Nanoscale* **2011**, *3* (3), 1084−1089.
(24) Bhise, A. B.; Late, D. J.; Sathe, B.; More, M. A.; Mulla, I. S.; Pillai, V. K.; Joag, D. S. Fabrication of In-Doped SnO_2 Nanowire Arrays and Its Field Emission Investigations. *J. Exp. Nanosci.* **2010**, *5* (6), 527−535.
(25) Bhise, A. B.; Late, D. J.; Sathe, B. R.; More, M. A.; Mulla, I. S.; Pillai, V. K.; Joag, D. S. Field Emission Investigation of Single Fe-Doped SnO_2 Wire. *Solid State Sci.* **2009**, *11* (6), 1114−1117.
(26) Bhise, A. B.; Late, D. J.; Ramgir, N. S.; More, M. A.; Mulla, I. S.; Pillai, V. K.; Joag, D. S. RuO_2 Doped SnO_2 Nanobipyramids on Si (100) As a Field Emitter. *Thin Solid Films* **2008**, *516* (18), 6388−6391.
(27) Bhise, A. B.; Late, D. J.; Ramgir, N. S.; More, M. A.; Mulla, I. S.; Pillai, V. K.; Joag, D. S. Field Emission Investigations of RuO_2-Doped SnO_2 wires. *Appl. Surf. Sci.* **2007**, *253* (23), 9159−9163.
(28) Bhise, A. B.; Late, D. J.; Walke, P. S.; More, M. A.; Pillai, V. K.; Mulla, I. S.; Joag, D. S. Sb-Doped SnO_2 Wire: Highly Stable Field Emitter. *J. Cryst. Growth* **2007**, *307* (1), 87−91.
(29) Ashok, B. B.; Dattatray, J. L.; Pravin, W.; Mahendra, A. M.; Imtiaz, S. M.; Vijayamohanan, K. P.; Dilip, S. J. A Single In-doped SnO_2 Submicrometre Sized Wire As a Field Emitter. *J. Phys. D: Appl. Phys.* **2007**, *40* (12), 3644.
(30) Faia, P. M.; Furtado, C. S.; Ferreira, A. J. Humidity Sensing Properties of a Thick-Film Titania Prepared by a Slow Spinning Process. *Sens. Actuators, B* **2004**, *101* (1−2), 183−190.
(31) Chitara, B.; Late, D. J.; Krupanidhi, S. B.; Rao, C. N. R. Room-Temperature Gas Sensors Based on Gallium Nitride Nanoparticles. *Solid State Commun.* **2010**, *150* (41−42), 2053−2056.
(32) Cuong, T. V.; Pham, V. H.; Chung, J. S.; Shin, E. W.; Yoo, D. H.; Hahn, S. H.; Huh, J. S.; Rue, G. H.; Kim, E. J.; Hur, S. H.; Kohl, P. A. Solution-Processed ZnO-Chemically Converted Graphene Gas Sensor. *Mater. Lett.* **2010**, *64* (22), 2479−2482.
(33) Zhu, X.; Zhu, Y.; Murali, S.; Stoller, M. D.; Ruoff, R. S. Nanostructured Reduced Graphene Oxide/Fe_2O_3 Composite As a High-Performance Anode Material for Lithium Ion Batteries. *ACS Nano* **2011**, *5* (4), 3333−3338.
(34) Zhu, X. J.; Hu, J.; Dai, H. L.; Ding, L.; Jiang, L. Reduced Graphene Oxide and Nanosheet-Based Nickel Oxide Microsphere Composite As an Anode Material for Lithium Ion Battery. *Electrochim. Acta* **2012**, *64* (0), 23−28.
(35) Hsieh, C. T.; Lin, J. S.; Chen, Y. F.; Teng, H. Pulse Microwave Deposition of Cobalt Oxide Nanoparticles on Graphene Nanosheets as Anode Materials for Lithium Ion Batteries. *J. Phys. Chem. C* **2012**, *116* (29), 15251−15258.
(36) Esfandiar, A.; Ghasemi, S.; Irajizad, A.; Akhavan, O.; Gholami, M. R. The Decoration of TiO_2/Reduced Graphene Oxide by Pd and Pt Nanoparticles for Hydrogen Gas Sensing. *Int. J. Hydrogen Energy* **2012**, *37* (20), 15423−15432.
(37) Wang, X.; Cao, X.; Bourgeois, L.; Guan, H.; Chen, S.; Zhong, Y.; Tang, D. M.; Li, H.; Zhai, T.; Li, L.; Bando, Y.; Golberg, D. N-Doped Graphene-SnO_2 Sandwich Paper for High-Performance Lithium-Ion Batteries. *Adv. Funct. Mater.* **2012**, *22* (13), 2682−2690.
(38) Yang, X.; Zhang, X.; Ma, Y.; Huang, Y.; Wang, Y.; Chen, Y. Superparamagnetic Graphene Oxide-Fe_3O_4 Nanoparticles Hybrid for Controlled Targeted Drug Carriers. *J. Mater. Chem.* **2009**, *19* (18), 2710−2714.
(39) Deng, S.; Tjoa, V.; Fan, H. M.; Tan, H. R.; Sayle, D. C.; Olivo, M.; Mhaisalkar, S.; Wei, J.; Sow, C. H. Reduced Graphene Oxide Conjugated Cu_2O Nanowire Mesocrystals for High-Performance NO_2 Gas Sensor. *J. Am. Chem. Soc.* **2012**, *134* (10), 4905−4917.
(40) Seo, S. D.; Lee, D. H.; Kim, J. C.; Lee, G. H.; Kim, D. W. Room-Temperature Synthesis of CuO/Graphene Nanocomposite Electrodes for High Lithium Storage Capacity. *Ceram. Int.* **2013**, *39* (2), 1749−1755.
(41) Mai, Y. J.; Wang, X. L.; Xiang, J. Y.; Qiao, Y. Q.; Zhang, D.; Gu, C. D.; Tu, J. P. CuO/Graphene Composite As Anode Materials for Lithium-Ion Batteries. *Electrochim. Acta* **2011**, *56* (5), 2306−2311.
(42) Zhao, B.; Liu, P.; Zhuang, H.; Jiao, Z.; Fang, T.; Xu, W.; Lu, B.; Jiang, Y. Hierarchical Self-Assembly of Microscale Leaf-Like CuO on Graphene Sheets for High-Performance Electrochemical Capacitors. *J. Mater. Chem. A* **2013**, *1* (2), 367−373.
(43) Sun, C. L.; Cheng, W. L.; Hsu, T. K.; Chang, C. W.; Chang, J. L.; Zen, J. M. Ultrasensitive and Highly Stable Nonenzymatic Glucose Sensor by a CuO/Graphene-Modified Screen-Printed Carbon Electrode Integrated with Flow-Injection Analysis. *Electrochem. Commun.* **2013**, *30* (0), 91−94.
(44) Gao, Y.; Li, Y.; Zhang, L.; Huang, H.; Hu, J.; Shah, S. M.; Su, X. Adsorption and Removal of Tetracycline Antibiotics from Aqueous Solution by Graphene Oxide. *J. Colloid Interface Sci.* **2012**, *368* (1), 540−546.
(45) Xu, C.; Wang, X.; Zhu, J.; Yang, X.; Lu, L. Deposition of Co_3O_4 Nanoparticles onto Exfoliated Graphite Oxide Sheets. *J. Mater. Chem.* **2008**, *18* (46), 5625−5629.
(46) Liu, S.; Tian, J.; Wang, L.; Luo, Y.; Sun, X. One-Pot Synthesis of CuO Nanoflower-Decorated Reduced Graphene Oxide and Its Application to Photocatalytic Degradation of Dyes. *Catal. Sci. Technol.* **2012**, *2* (2), 339−344.
(47) Cuong, T. V.; Pham, V. H.; Tran, Q. T.; Hahn, S. H.; Chung, J. S.; Shin, E. W.; Kim, E. J. Photoluminescence and Raman Studies of Graphene Thin Films Prepared by Reduction of Graphene Oxide. *Mater. Lett.* **2010**, *64* (3), 399−401.
(48) Zhu, J.; Zeng, G.; Nie, F.; Xu, X.; Chen, S.; Han, Q.; Wang, X. Decorating Graphene Oxide with CuO Nanoparticles in a Water-Isopropanol System. *Nanoscale* **2010**, *2* (6), 988−994.

(49) Ko, J. W.; Kim, S. W.; Hong, J.; Ryu, J.; Kang, K.; Park, C. B. Synthesis of Graphene-Wrapped CuO Hybrid Materials by CO_2 Mineralization. *Green Chem.* **2012**, *14* (9), 2391−2394.
(50) Wang, W. C.; Tian, Y. T.; Li, K.; Lu, E. Y.; Gong, D. S.; Li, X. J. Capacitive Humidity-Sensing Properties of Zn_2SiO_4 Film Grown on Silicon Nanoporous Pillar Array. *Appl. Surf. Sci.* **2013**, *273* (0), 372−376.
(51) Wang, Z.; Lu, Y.; Yuan, S.; Shi, L.; Zhao, Y.; Zhang, M.; Deng, W. Hydrothermal Synthesis and Humidity Sensing Properties of Size-Controlled Zirconium Oxide (ZrO_2) Nanorods. *J. Colloid Interface Sci.* **2013**, *396* (0), 9−15.
(52) Su, P. G.; Hsu, H. C.; Liu, C. Y. Layer-by-layer Anchoring of Copolymer of Methyl Methacrylate and [3-(Methacrylamino)propyl] Trimethyl Ammonium Chloride to Gold Surface on Flexible Substrate for Sensing Humidity. *Sens. Actuators, B* **2013**, *178* (0), 289−295.
(53) Ghosh, A.; Late, D. J.; Panchakarla, L. S.; Govindaraj, A.; Rao, C. N. R. NO_2 and Humidity Sensing Characteristics of Few-Layer Graphenes. *J. Exp. Nanosci.* **2009**, *4* (4), 313−322.
(54) Late, D. J.; Huang, Y. K.; Liu, B.; Acharya, J.; Shirodkar, S. N.; Luo, J.; Yan, A.; Charles, D.; Waghmare, U. V.; Dravid, V. P.; Rao, C. N. R. Sensing Behavior of Atomically Thin-Layered MoS_2 Transistors. *ACS Nano* **2013**, *7* (6), 4879−4891.
(55) Late, D. J.; Liu, B.; Matte, H. S. S. R.; Dravid, V. P.; Rao, C. N. R. Hysteresis in Single-Layer MoS_2 Field Effect Transistors. *ACS Nano* **2012**, *6* (6), 5635−5641.
(56) Lu, Y.; Wang, Z.; Yuan, S.; Shi, L.; Zhao, Y.; Deng, W. Microwave-Hydrothermal Synthesis and Humidity Sensing Behavior of ZrO_2 Nanorods. *RSC Adv.* **2013**, *3* (29), 11707−11714.
(57) Yeow, J. T. W.; She, J. P. M. Carbon Nanotube-Enhanced Capillary Condensation for a Capacitive Humidity Sensor. *Nanotechnology* **2006**, *17* (21), 5441.
(58) Liao, L.; Zhang, Z.; Yan, B.; Zheng, Z.; Bao, Q. L.; Wu, T.; Li, C. M.; Shen, Z. X.; Zhang, J. X.; Gong, H.; Li, J. C.; Yu, T. Multifunctional CuO Nanowire Devices: p-Type Field Effect Transistors and CO Gas Sensors. *Nanotechnology* **2009**, *20* (8), 085203.
(59) Yu, Y. J.; Zhao, Y.; Ryu, S.; Brus, L. E.; Kim, K. S.; Kim, P. Tuning the Graphene Work Function by Electric Field Effect. *Nano Lett.* **2009**, *9* (10), 3430−3434.
(60) Zhou, K.; Zhu, Y.; Yang, X.; Jiang, X.; Li, C. Preparation of Graphene-TiO_2 Composites with Enhanced Photocatalytic Activity. *New J. Chem.* **2011**, *35* (2), 353−359.
(61) Sellappan, R.; Sun, J.; Galeckas, A.; Lindvall, N.; Yurgens, A.; Kuznetsov, A. Y.; Chakarov, D. Influence of Graphene Synthesizing Techniques on the Photocatalytic Performance of Graphene-TiO_2 Nanocomposites. *Phys. Chem. Chem. Phys.* **2013**, *15* (37), 15528−15537.
(62) Nie, B.; Hu, J. G.; Luo, L. B.; Xie, C.; Zeng, L. H.; Lv, P.; Li, F. Z.; Jie, J. S.; Feng, M.; Wu, C. Y.; Yu, Y. Q.; Yu, S. H. Monolayer Graphene Film on ZnO Nanorod Array for High-Performance Schottky Junction Ultraviolet Photodetectors. *Small* **2013**, *9* (17), 2872−2879.
(63) Zhang, Z.; Zou, R.; Song, G.; Yu, L.; Chen, Z.; Hu, J. Highly Aligned SnO_2 Nanorods on Graphene Sheets for Gas Sensors. *J. Mater. Chem.* **2011**, *21* (43), 17360−17365.
(64) Zhang, N.; Zhang, Y.; Pan, X.; Yang, M. Q.; Xu, Y. J. Constructing Ternary CdS−Graphene−TiO_2 Hybrids on the Flatland of Graphene Oxide with Enhanced Visible-Light Photoactivity for Selective Transformation. *J. Phys. Chem. C* **2012**, *116* (34), 18023−18031.
(65) Fan, G.; Zhu, H.; Wang, K.; Wei, J.; Li, X.; Shu, Q.; Guo, N.; Wu, D. Graphene/Silicon Nanowire Schottky Junction for Enhanced Light Harvesting. *ACS Appl. Mater. Interfaces* **2011**, *3* (3), 721−725.
(66) Lin, J.; Hu, P.; Zhang, Y.; Fan, M.; He, Z.; Ngaw, C. K.; Loo, J. S. C.; Liao, D.; Tan, T. T. Y. Understanding the Photoelectrochemical Properties of a Reduced Graphene Oxide-WO_3 Heterojunction Photoanode for Efficient Solar-Light-Driven Overall Water Splitting. *RSC Adv.* **2013**, *3* (24), 9330−9336.